

Terahertz photoresistivity of a high-mobility 3D topological insulator based on a strained HgTe film

M. L. Savchenko,^{1,2, a)} M. Otteneder,³ S. D. Ganichev,^{3, b)} N. N. Mikhailov,^{1,2} and Z. D. Kvon^{1,2}

¹⁾Rzhanov Institute of Semiconductor Physics, Novosibirsk 630090, Russia

²⁾Novosibirsk State University, Novosibirsk 630090, Russia

³⁾Terahertz Center, University of Regensburg, 93040 Regensburg, Germany

(Dated: 19 August 2020)

We report on a detailed study of the terahertz (THz) photoresistivity in a strained HgTe three-dimensional topological insulator (3D TI) for all Fermi level positions: inside the conduction and valence bands, and in the bulk gap. In the presence of magnetic field we detect a resonance corresponding to the cyclotron resonance (CR) in the top surface Dirac fermions (DF) and examine the nontrivial dependence of the surface state cyclotron mass on the Fermi level position. We also detect additional resonant features at moderate electron densities and demonstrate that they are caused by the mixing of surface DF and bulk electrons. At high electron densities, we observe THz radiation induced $1/B$ -periodic low-field magneto-oscillations coupled to harmonics of the CR and demonstrate that they have a common origin with microwave-induced resistance oscillations (MIRO) previously observed in high mobility GaAs-based heterostructures.

Three-dimensional TIs based on strained HgTe films have been the subject of an intensive study in the last ten years. This system is a strong topological insulator with electronic properties mediated by conducting surface helical states with close to linear dispersion with spins locked to the electron's momentum^{1,2} and is characterized by a very high mobility of the surface DF, reaching $5 \times 10^5 \text{ cm}^2/\text{Vs}$ in these systems, and low bulk conductivity. The properties of the surface states have been comprehensively studied using magneto-transport, phase-sensitive SQUID and capacitance spectroscopy³⁻¹¹. These experiments resulted in the observation of the quantum Hall effect and probing of quantum capacitance in a 3D topological insulator, demonstrated a non-trivial Berry phase of Shubnikov – de Haas oscillations in transport and capacitance responses, provided an access to a detailed study of the surface states transport properties, and demonstrated highly efficient spin-to-charge current conversion. Presence of the topologically protected conducting surface states in strained HgTe 3D TIs also gives rise to a number of phenomena driven by THz electric fields. Observation of universal Faraday and Kerr effects^{12,13} predicted in Ref. 14; THz quantum Hall effect¹⁵ and photogalvanic currents^{16,17} excited in the surface states; study of surface states dynamic applying time domain spectroscopy¹⁸ and cyclotron resonance spectroscopy^{15-17,19}, where values of the effective mass of DF from top and bottom surfaces were determined, are only some examples of the achievements in this field.

While THz radiation induced optical and photocurrent phenomena have been widely investigated there has been no work so far aimed at the study of the photoconductive (photoresistive) response of the surface states. Such measurements, however, would not only yield information on tiny details of carrier scattering mechanisms and CR (for HgTe 2D systems see Ref. 20) but also may result in the observation of novel phenomena in 3D TI, such as, e.g., MIRO previously detected in

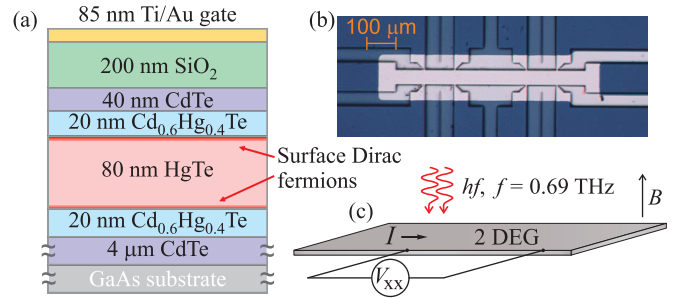


FIG. 1. (a) Schematic cross section of the structure under study. Bright red lines represent surface DF on the top and bottom surfaces of the HgTe film. (b) Optical micrograph of the device; faint lilac area corresponds to the gated region. (c) Schematic experimental setup.

2D systems with parabolic dispersion^{21,22} and, most recently, in DF in graphene²³.

In this paper we report on the investigation of the THz photoresistance of HgTe-based 3D TIs for all Fermi level, E_F , positions: inside the conduction and valence bands, and in the bulk energy gap. Studying the magnetic field dependences of the photoresponse we observed pronounce CR and, at high electron densities, THz radiation induced MIRO-like oscillations coupled to CR. Furthermore, for the intermediate electron densities we detected an additional set of oscillations which behave similarly to magneto-intersubband oscillations (MISO) detected in coupled double quantum wells (QWs)^{24,25}.

Experimental samples are field effect transistor-like Hall-bar structures with semi-transparent Ti/Au gates fabricated on the basis of strained 80-nm HgTe films that have been grown by molecular beam epitaxy on a GaAs (013) substrate⁴ (Fig. 1). The Hall-bar channel width is $50 \mu\text{m}$ and distances between potential probes are 100 and $250 \mu\text{m}$. The samples are placed into an optical cryostat. We apply a molecular far-infrared laser as a source of THz radiation with frequency $f = 0.69 \text{ THz}$ (wavelength $\lambda = 432 \mu\text{m}$)^{26,27}. The incident power $P \approx 20 \text{ mW}$ is modulated at about 160 Hz by

^{a)}Electronic mail: mlsavchenko@isp.nsc.ru

^{b)}Electronic mail: sergey.ganichev@physik.uni-regensburg.de

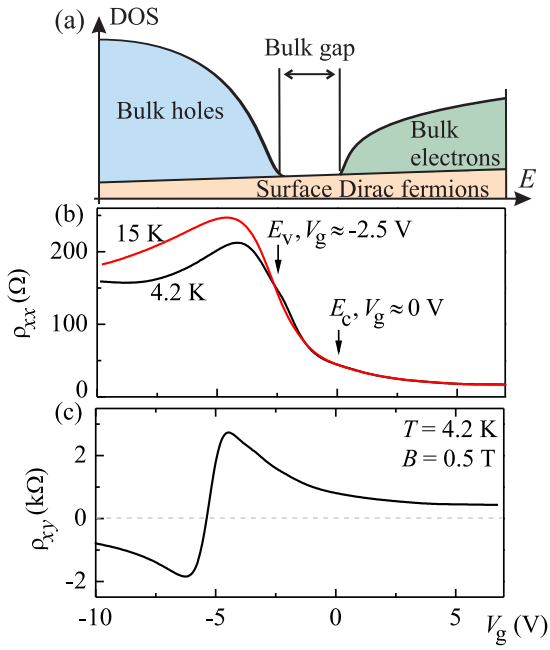


FIG. 2. (a) Schematic energy dependence of the density of states (DOS) of the system under study. (b) Gate voltage dependence of dissipative resistivity $\rho_{xx}(V_g)$ measured at $T = 4.2$ K (black) and $T = 15$ K (red). (c) Gate voltage dependence of the Hall resistivity $\rho_{xy}(V_g)$ measured at $B = 0.5$ T and $T = 4.2$ K.

an optical chopper. Photoresistance is measured by means of a double modulation technique²⁸ with a low modulation frequency of 6 Hz and a high one corresponding to the chopper frequency. The temperature range of the experiment is (2 – 20) K.

All studied samples have been characterized by magneto-transport measurements using a standard low-frequency lock-in technique in a perpendicular magnetic field B up to 7 T and current I in the range of (10 – 100) nA. Typical gate voltage dependences of dissipative, $\rho_{xx}(V_g)$, and Hall, $\rho_{xy}(V_g)$, resistivities are shown in Fig. 2 (b) and (c). Using $\rho_{xx}(V_g)$ one can determine the gate voltages corresponding to the conduction band bottom and the valence band top⁴, see arrows in Fig. 2.

Fig. 3 (a) demonstrates the main result of our work – magnetic field dependences of the photoresistivity $\delta\rho_{ph}(B)$ normalized to the maximum of its absolute value $|\delta\rho_{ph}^{\max}|$. The dependences are measured at $\lambda = 432\mu\text{m}$ for three ranges of V_g corresponding to the Fermi level position in: i) the valence band ($V_g < -2.5$ V), ii) in the gap (-2.5 V $< V_g < 0$ V), and iii) in the conduction band ($V_g > 0$ V). All curves are measured at 20 K. This temperature is high enough to suppress the contribution of the Shubnikov – de Haas oscillations. One can clearly see that $\rho_{ph}/|\rho_{ph}^{\max}|(B)$ dependences have resonant shapes with the maximum position lying in the magnetic field range $B_{CR} = (0.7 - 0.9)$ T depending on the applied gate voltage, i.e., Fermi level position. Using the value of B_{CR} one can determine the cyclotron effective mass $m_c = eB_{CR}/(2\pi f)$, where $e > 0$ is the elementary charge. In Fig. 3 (b) we show the gate voltage dependence of m_c . One can see that this de-

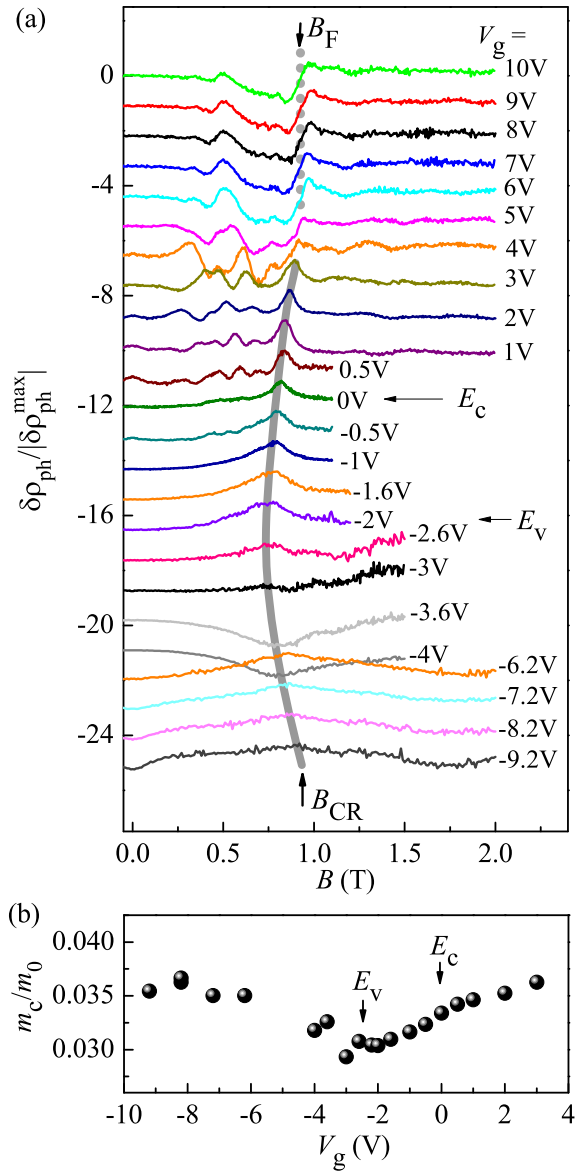


FIG. 3. (a) Magnetic field dependences of the normalized photoresistivity $\delta\rho_{ph}/|\delta\rho_{ph}^{\max}|(B)$ measured at different gate voltages, corresponding to the position of the Fermi level in the bulk valence band ($V_g < -2.5$ V), inside the bulk gap (-2.5 V $< V_g < 0$ V), and in the bulk conduction band ($V_g > 0$ V). The curves are vertically shifted by -1.1 for clarity. Thick solid and dotted gray lines schematically correspond to the CR positions B_{CR} and the fundamental frequency B_F (see Eq. (3)). (b) Gate voltage dependence of the obtained cyclotron mass.

pendence has a nonmonotonic behavior with a minimum value of $m_c = 0.03 m_0$ near the valence band top; m_0 is the free electron mass. The cyclotron mass approaches its maximum value $m_c = 0.04 m_0$ at the highest gate voltages, corresponding to a DF density of about $7 \times 10^{11} \text{ cm}^{-2}$. In fact, such nonmonotonic behavior of the cyclotron mass and its values are in line to what was measured^{12,16,19}, and calculated^{16,19} for surface DF in HgTe.

The temperature dependence of the resistance (not shown)

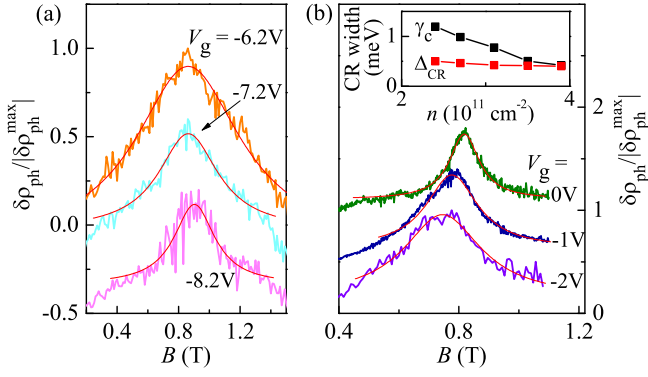


FIG. 4. Examples of the Lorentzian fitting of the normalized photoresistivity measured when the Fermi level is in the bulk valence band (a) and inside the bulk gap (b). Red curves are Lorentzian fits of CR. *Inset* – Density dependence of the experimental cyclotron width γ_c (black) and the theoretical cyclotron width for separated Landau levels Δ_{CR} (red) for E_F positions inside the bulk energy gap.

indicate that at all gate voltages the photoresistivity sign observed under resonance conditions corresponds to carrier heating. Then, it can be expressed as

$$\delta\rho_{ph} = \alpha A (dR/dT), \quad (1)$$

where A is the proportionality coefficient relating the incident power to the change in the temperature of the DF and α is the absorption coefficient. As one can see from this expression the properties of the photoresistivity are expected to be determined primarily by the behavior of the absorption coefficient.

Now we analyze the shape the CR photoresistivity. We begin from a gate voltage range corresponding to the Fermi level positions in the valence band (see Fig. 4 (a)). In this range the photoresistivity is quite satisfactory fitted by a Lorentzian curve. It is interesting to compare the Lorentzian width γ_c with the theoretical CR width Δ_{CR} for separated Landau levels using a well-known expression for the latter in the case of a short range potential^{22,29}

$$\Delta_{CR}^2 = (2/\pi)\hbar\omega_c(\hbar/\tau), \quad (2)$$

where ω_c is the cyclotron frequency and τ is the transport relaxation time. In the valence band the DF mobility is about $2 \times 10^5 \text{ cm}^2/\text{Vs}$ which corresponds to $\Delta_{CR} \approx 0.6 \text{ meV}$. This value is two to three times larger compared to experimental resonance width γ_c values. It is likely that the origin of the indicated discrepancy is the inelastic scattering of surface DF by bulk holes which is very significant in the temperature range we used in our experiments⁴. As a result the CR width is determined by principally different scattering processes: elastic impurity scattering and inelastic electron-hole one.

Next we consider the CR photoresistivity shape when the Fermi level enters into the gap (Fig. 4 (b)). The fitting of the photoresistivity by a Lorentzian function also demonstrates quite good agreement. It gives a resonance width of about 0.3 T when the Fermi level lies near the top of the valence band, and it decreases when the Fermi level moves to the bottom of the conduction band. More careful analysis of the γ_c

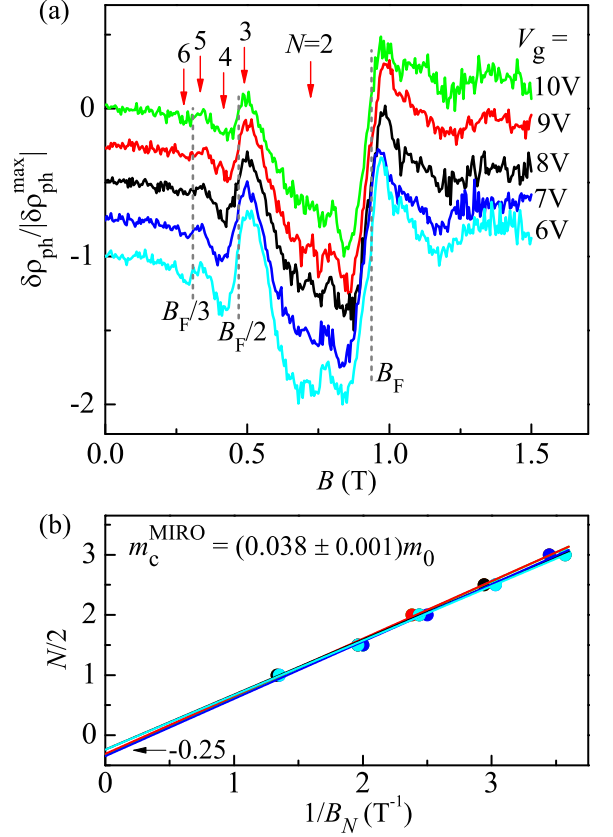


FIG. 5. (a) Magnetic field dependences of the normalized photoresistivity $\delta\rho_{ph}/|\delta\rho_{ph}^{\max}|$ measured at $V_g = 6, 7, 8, 9,$ and 10 V as also shown in Fig. 3 (a). Traces are vertically shifted by -0.25 for clarity. (b) The reciprocal magnetic field dependence of the photoresistivity extrema that are indicated by arrows and numbered as $N = 2, 3, \dots$. The symbols and approximation lines have the same color code as the corresponding photoresistivity curves.

behavior shows an interesting feature (inset to Fig. 4 (b)): as the Fermi level moves through the gap from the valence band top to the conduction band bottom a significant CR peak narrowing occurs, while Δ_{CR} has no change. This indicates that the shape of the surface Dirac fermion CR is determined not only by the transport relaxation time as it is the case in text book 3D cases, see Eq. (2). It is well-known that there is a topological back scattering protection in 3D TIs, but in contrast to two-dimensional TIs this protection does not work for the scattering on finite angles and therefore only weakly changes τ . To explain this fact one can assume that, in contradiction to the transport relaxation time, the CR lifetime is much more sensitive to the topological back scattering protection that plays a more important role as the DF momentum becomes larger.

As the Fermi level leaves the gap and enters the conduction band (see a $\delta\rho_{ph}/|\delta\rho_{ph}^{\max}|(B)$ dependence in Fig. 3 (a) at $V_g = 0.5 \text{ V}$) photoresistivity oscillations at magnetic fields below B_{CR} emerge. Note that these oscillations are absent when the Fermi level intersects only the surface states. Since the top surface DF have higher density and mobility in the stud-

ied systems^{4,7}, the oscillations are presumably generated by the mixing of a top surface DF band and the bulk conduction band, which, more accurately, contains a set of the size-quantized subbands^{3,16}. So the observed oscillations are similar to magnetointersubband oscillations (MISO) in coupled double QWs studied in Ref. 24 and 25. But in our case we have two significantly different sets of interacted bands: the spin-polarized surface DF band and the size-quantized subbands of the 80 nm HgTe film. Moreover, in our experiment we have an important advantage: due to the field effect transistor structure we are able to change the position of the Fermi level and correspondingly the subband densities.

As the Fermi level moves further inside the conduction band, these oscillations are superimposed with THz induced MIRO-like oscillations that have nearly the same structure for several gate voltages ranging from 6 to 10 V, see Fig. 5 (a). Arrows in this figure show the positions of subsequent extrema of MIRO, numbered as $N = 2, 3, \dots$. It is well known that for MIRO^{22,23}

$$\delta\rho_{\text{ph}} \propto -\sin(2\pi B_F/B), \quad (3)$$

where $B_F = 2\pi f m_c^{\text{MIRO}}/e$. Thereby, the slope of the $N/2$ v.s. B^{-1} dependence, see Fig. 5 (b), is equal to B_F that allows us to determine the corresponding effective mass $m_c^{\text{MIRO}} = (0.038 \pm 0.001)m_0$. This value is close to the cyclotron mass values at high positive V_g , where it is possible to mark out CR ($V_g = 2$ and 3 V). We note that approximation lines $N/2(B^{-1})$ start near $N/2 = -0.25$ as it is predicted for MIRO²². The detailed study of the observed transformation of the photoresistance from one CR peak to MIRO-like oscillations through a rich picture of interband interaction induced oscillations will be reported later.

To conclude, we have observed and studied the THz cyclotron resonance photoresistivity of 80-nm-thick strained HgTe 3D TI. The photoresistivity was studied at all Fermi level positions: inside the conduction and valence bands and in the bulk gap. For the Fermi level lying in the valence band or the gap, we observed a single resonance of the photoresistivity, which is caused by the cyclotron resonance of DF in the top surface. For higher positions of the Fermi level, i.e. for E_F lying in the conduction band, the CR-photoresistivity becomes superimposed first with magnetointersubband oscillations, and, at further increase of E_F , with MIRO oscillations.

ACKNOWLEDGMENTS

We are grateful to Ivan Dmitriev for discussions. Novosibirsk team acknowledges the financial support by the Russian Science Foundation (Grant No. 16-12-10041-P). M. Otteneder and S.D. Ganichev gratefully acknowledge the support of the Deutsche Forschungsgemeinschaft (DFG) - Project-ID 314695032 - SFB 1277, and the Volkswagen Stiftung Program (97738). S.D.G. also thanks the IRAP program of the Foundation for Polish Science (grant MAB/2018/9, CENTERA) for the support.

DATA AVAILABILITY

The data that support the findings of this study are available from the corresponding authors upon reasonable request.

- ¹L. Fu and C. L. Kane, *Phys. Rev. B* **76**, 045302 (2007).
- ²X. Dai, T. L. Hughes, X. L. Qi, Z. Fang, and S. C. Zhang, *Phys. Rev. B* **77**, 125319 (2008).
- ³C. Brüne, C. X. Liu, E. G. Novik, E. M. Hankiewicz, H. Buhmann, Y. L. Chen, X. L. Qi, Z. X. Shen, S. C. Zhang, and L. W. Molenkamp, *Phys. Rev. Lett.* **106**, 126803 (2011).
- ⁴D. A. Kozlov, Z. D. Kvon, E. B. Olshanetsky, N. N. Mikhailov, S. A. Dvoretzky, and D. Weiss, *Phys. Rev. Lett.* **112**, 196801 (2014).
- ⁵C. Brüne, C. Thienel, M. Stüiber, J. Böttcher, H. Buhmann, E. G. Novik, C.-X. Liu, E. M. Hankiewicz, and L. W. Molenkamp, *Phys. Rev. X* **4**, 041045 (2014).
- ⁶L. Maier, E. Bocquillon, M. Grimm, J. B. Oostinga, C. Ames, C. Gould, C. Brüne, H. Buhmann, and L. W. Molenkamp, *Phys. Scr.* **T164**, 014002 (2015).
- ⁷D. A. Kozlov, D. Bauer, J. Ziegler, R. Fischer, M. L. Savchenko, Z. D. Kvon, N. N. Mikhailov, S. A. Dvoretzky, and D. Weiss, *Phys. Rev. Lett.* **116**, 166802 (2016).
- ⁸H. Maier, J. Ziegler, R. Fischer, D. Kozlov, Z. D. Kvon, N. Mikhailov, S. A. Dvoretzky, and D. Weiss, *Nat. Commun.* **8**, 2023 (2017).
- ⁹C. Thomas, O. Crauste, B. Haas, P.-H. Jouneau, C. Bäuerle, L. P. Lévy, E. Orignac, D. Carpentier, P. Ballet, and T. Meunier, *Phys. Rev. B* **96**, 245420 (2017).
- ¹⁰J. Ziegler, R. Kozlovsky, C. Gorini, M.-H. Liu, S. Weishäupl, H. Maier, R. Fischer, D. A. Kozlov, Z. D. Kvon, N. Mikhailov, S. A. Dvoretzky, K. Richter, and D. Weiss, *Phys. Rev. B* **97**, 035157 (2018).
- ¹¹P. Noel, C. Thomas, Y. Fu, L. Vila, B. Haas, P.-H. Jouneau, S. Gambarelli, T. Meunier, P. Ballet, and J. P. Attané, *Phys. Rev. Lett.* **120**, 167201 (2018).
- ¹²A. M. Shuvaev, G. V. Astakhov, C. Brüne, H. Buhmann, L. W. Molenkamp, and A. Pimenov, *Semicond. Sci. Technol.* **27**, 124004 (2012).
- ¹³V. Dziom, A. Shuvaev, A. Pimenov, G. V. Astakhov, C. Ames, K. Bendias, J. Böttcher, G. Tkachov, E. M. Hankiewicz, C. Brüne, H. Buhmann, and L. W. Molenkamp, *Nat. Commun.* **8**, 15197 (2017).
- ¹⁴W.-K. Tse and A. H. MacDonald, *Phys. Rev. Lett.* **105**, 057401 (2010).
- ¹⁵A. M. Shuvaev, G. V. Astakhov, G. Tkachov, C. Brüne, H. Buhmann, L. W. Molenkamp, and A. Pimenov, *Phys. Rev. B* **87**, 121104(R) (2013).
- ¹⁶K. M. Dantscher, D. A. Kozlov, P. Olbrich, C. Zoth, P. Faltermeier, M. Lindner, G. V. Budkin, S. A. Tarasenko, V. V. Bel'kov, Z. D. Kvon, N. N. Mikhailov, S. A. Dvoretzky, D. Weiss, B. Jenichen, and S. D. Ganichev, *Phys. Rev. B* **92**, 165314 (2015).
- ¹⁷S. Candussio, G. V. Budkin, M. Otteneder, D. A. Kozlov, I. A. Dmitriev, V. V. Bel'kov, Z. D. Kvon, N. N. Mikhailov, S. A. Dvoretzky, and S. D. Ganichev, *Phys. Rev. Mater.* **3**, 054205 (2019).
- ¹⁸J. N. Hancock, J. L. M. van Mechelen, A. B. Kuzmenko, D. van der Marel, C. Brüne, E. G. Novik, G. V. Astakhov, H. Buhmann, and L. W. Molenkamp, *Phys. Rev. Lett.* **107**, 136803 (2011).
- ¹⁹J. Gospodarič, V. Dziom, A. Shuvaev, A. A. Dobretsova, N. N. Mikhailov, Z. D. Kvon, and A. Pimenov, *Phys. Rev. B* **99**, 115130 (2019).
- ²⁰M. Otteneder, I. A. Dmitriev, S. Candussio, M. L. Savchenko, D. A. Kozlov, V. V. Bel'kov, Z. D. Kvon, N. N. Mikhailov, S. A. Dvoretzky, and S. D. Ganichev, *Phys. Rev. B* **98**, 245304 (2018).
- ²¹M. A. Zudov, R. R. Du, J. A. Simmons, and J. L. Reno, *Phys. Rev. B* **64**, 201311 (2001).
- ²²I. A. Dmitriev, A. D. Mirlin, D. G. Polyakov, and M. A. Zudov, *Rev. Mod. Phys.* **84**, 1709 (2012).
- ²³E. Mönch, D. A. Bandurin, I. A. Dmitriev, I. Y. Phinney, I. Yahniuk, T. Taniguchi, K. Watanabe, P. Jarillo-Herrero, and S. D. Ganichev, *Nano Lett.* **20**, 5943 (2020).
- ²⁴A. A. Bykov, D. R. Islamov, A. V. Goran, and A. I. Toropov, *JETP Lett.* **87**, 477 (2008).
- ²⁵S. Wiedmann, G. M. Gusev, O. E. Raichev, T. E. Lamas, A. K. Bakarov, and J. C. Portal, *Phys. Rev. B* **78**, 121301 (2008).
- ²⁶Z.-D. Kvon, S. N. Danilov, N. N. Mikhailov, S. A. Dvoretzky, W. Prettl, and S. D. Ganichev, *Phys. E* **40**, 1885 (2008).

- ²⁷P. Olbrich, C. Zoth, P. Vierling, K.-M. Dantscher, G. V. Budkin, S. A. Tarasenko, V. V. Bel'kov, D. A. Kozlov, Z. D. Kvon, N. N. Mikhailov, S. A. Dvoretzky, and S. D. Ganichev, *Phys. Rev. B* **87**, 235439 (2013).
- ²⁸D. A. Kozlov, Z. D. Kvon, N. N. Mikhailov, S. A. Dvoretzky, and J. C. Portal, *JETP Lett.* **93**, 170 (2011).
- ²⁹T. Ando, A. B. Fowler, and F. Stern, *Rev. Mod. Phys.* **54**, 437 (1982).